Molecular Therapy
Oncolytics
Original Article

# Treatment of glioblastoma with current oHSV variants reveals differences in efficacy and immune cell recruitment

Joseph W. Jackson,[1] Bonnie L. Hall,[1] Marco Marzulli,[1] Vrusha K. Shah,[1] Lisa Bailey,[1] E. Antonio Chiocca,[2] William F. Goins,[1] Gary Kohanbash,[3] Justus B. Cohen,[1] and Joseph C. Glorioso[1]

[1]Department of Microbiology and Molecular Genetics, University of Pittsburgh, School of Medicine, Pittsburgh, PA 15219, USA; [2]Harvey W. Cushing Neuro-oncology Laboratories (HCNL), Department of Neurosurgery, Harvard Medical School and Brigham and Women's Hospital, Boston, MA 02115, USA; [3]Department of Neurological Surgery, University of Pittsburgh School of Medicine, Pittsburgh, PA 15219, USA

**Oncolytic herpes simplex viruses (oHSVs) have demonstrated efficient lytic replication in human glioblastoma tumors using immunodeficient mouse models, but early-phase clinical trials have reported few complete responses. Potential reasons for the lack of efficacy are limited vector potency and the suppressive glioma tumor microenvironment (TME). Here we compare the oncolytic activity of two HSV-1 vectors, a KOS-strain derivative KG4:T124 and an F-strain derivative rQNestin34.5v.1, in the CT2A and GL261N4 murine syngeneic glioma models. rQNestin34.5v1 generally demonstrated a greater *in vivo* viral burden compared to KG4:T124. However, both vectors were rapidly cleared from CT2A tumors, while virus remained ensconced in GL261N4 tumors. Immunological evaluation revealed that the two vectors induced similar changes in immune cell recruitment to either tumor type at 2 days after infection. However, at 7 days after infection, the CT2A microenvironment displayed the phenotype of an untreated tumor, while GL261N4 tumors exhibited macrophage and $CD4^+/CD8^+$ T cell accumulation. Furthermore, the CT2A model was completely resistant to virus therapy, while in the GL261N4 model rQNestin34.5v1 treatment resulted in enhanced macrophage recruitment, impaired tumor progression, and long-term survival of a few animals. We conclude that prolonged intratumoral viral presence correlates with immune cell recruitment, and both are needed to enhance anti-tumor immunity.**

## INTRODUCTION

Glioblastoma multiforme (GBM) is a common brain cancer, with a devastating median patient survival of ~15 months.[1–3] The standard treatment for GBM patients is characteristically tumor resection followed by chemo- and/or radiotherapy.[4] While median patient survival has increased marginally in recent decades,[5] truly effective therapies remain elusive, pointing to an urgent need for novel treatments. In 2015, an oncolytic herpes simplex virus (oHSV) became the first US Food and Drug Administration (FDA)-approved oncolytic virus for cancer treatment, highlighting the promise of HSV-based approaches.[6] Indeed, several oHSV designs are currently in clinical trial to treat GBM, but early-phase results report few complete responses and little evidence that oHSV treatment can impede tumor recurrence following single-dose vector administration.[7] Here, we mimic clinical investigations using immunocompetent pre-clinical mouse models in an effort to better understand whether single-dose administration of oHSV can induce durable viral replication and spread resulting in widespread tumor killing and immune cell recruitment and activation.

We compared the oncolytic activity of two oHSV vectors that are early derivatives of oHSV vectors, which are currently in clinical trials for solid tumors or specifically GBM. Furthermore, both vectors used herein retain copies of the HSV neurovirulence gene ICP34.5, which is deleted in the majority of other oHSV designs.[8] The first vector is rQNestin34.5v.1, an oncolytic HSV-1 F-strain derivative that was attenuated by deleting both copies of the neurovirulence gene ICP34.5 and reconstituting single-copy ICP34.5 expression using a tumor-specific nestin-promoter-driven ICP34.5 cassette[9] (Figure 1); nestin is highly expressed in a variety of cancers, including human GBM.[10] Lack of ICP34.5 renders HSV avirulent in the brain and greatly hinders overall viral replication in non-tumor cells.[11] Thus, these modifications in rQNestin34.5v.1 expression enabled viral replication within the tumor, while ensuring safety if unintended cellular targets become infected. rQNestin34.5v1 has a GFP cassette fused to the HSV infected cell protein 6 (ICP6), while rQNestin34.5v2 is deleted for the GFP cassette[12] and is currently in a phase 1 clinical trial for GBM (ClinicalTrials.gov: NCT03152318). The second vector is KG4:T124, an HSV-1 KOS-strain derivative that is deleted for the reiterated sequences ("joint") separating the $U_L$ and $U_S$ unique genome components and is blocked for replication in normal neurons due to the incorporation of four copies of a recognition sequence for miR-124 in the 3′ UTR of the essential virus gene ICP4[13] (Figure 1);

Received 3 May 2021; accepted 17 July 2021;
https://doi.org/10.1016/j.omto.2021.07.009.

**Correspondence:** Joseph C. Glorioso, Department of Microbiology and Molecular Genetics, University of Pittsburgh, School of Medicine, Pittsburgh, PA 15219, USA.
**E-mail:** glorioso@pitt.edu

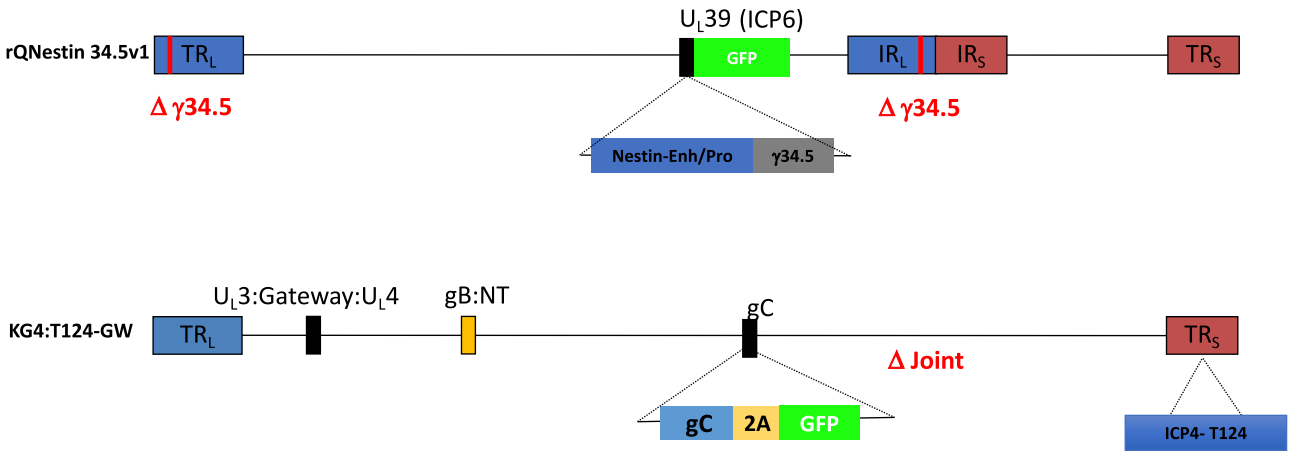


**Figure 1. Depiction of rQNestin34.5v1 and KG4:T124 genetic alterations**

miR-124 expression is significantly downregulated in GBM but highly expressed in healthy neurons.[14] KG4:T124 also contains a double point mutation in the glycoprotein B gene that increases the rate of viral entry,[15] and glycoprotein C is linked to a GFP cassette via a T2A self-cleaving peptide.[15] An armed derivative of the KOS vector (ONCR-177) is being used in a phase I clinical trial to treat solid tumors (ClinicalTrials.gov: NCT04348916).

Since both of these oHSVs are in clinical trials for human tumors, but only rQNestin34.5v2 is in a trial for GBM while ONCR-177 is in solid tumors, we hypothesized that a comparative effort could lead one to decide if a KG4:T124 derivate could be utilized for GBM and potentially vice versa. Our goal was to determine whether either vector showed replication or anti-tumor advantages using the CT2A and GL261N4 murine syngeneic glioma models.[16,17] The GL261N4 model is a derivative of the GL261 cell line that has been engineered to express human nectin-1.[16] Parental GL261 cells that lack human nectin-1 are non-permissive for HSV replication, while CT2A cells support HSV replication without the addition of human nectin-1.[18] The CT2A glioma model is immunologically inert and represents a more immunosuppressive[19] and aggressive syngeneic model than GL261N4.[17] These immune-competent GBM models were used to monitor *in vivo* oHSV replication dynamics, immune cell recruitment to the tumor following treatment, and the ability of oHSV to limit tumor progression and improve animal survival. We hypothesized that the duration and magnitude of oHSV replication *in vivo* would correlate with increased immune cell recruitment to the tumor, thereby limiting tumor progression. Our results showed that both prolonged virus presence within the tumor and virus-induced immune cell activity are needed to induce protective anti-tumor responses.

## RESULTS

### oHSV replication in the CT2A and GL261N4 murine syngeneic glioma models

The oHSV vectors KG4:T124 and rQNestin34.5v1 have been previously described.[9,13] We performed whole-genome sequencing on both KG4:T124 and rQNestin34.5v1 to confirm the genetic stability of either vector following production (data not shown). *In vitro* analyses analyzing oHSV entry, replication, and oncolytic capacity in the mouse CT2A and GL261N4 cells were performed (Figures S1A–S1C). KG4:T124 demonstrated slightly more efficient viral entry compared to rQNestin34.5v1, but overall rQNestin34.5v1 replicated more efficiently and induced greater cell death than KG4:T124 *in vitro*. Neither vector displayed preferred affinity for a particular cell line and demonstrated similar *in vitro* replication kinetics in both models. Next, we sought to determine whether the replication differences observed *in vitro* translated *in vivo*. HSV replication kinetics *in vivo* were mapped over time for each vector in both models. Animals were intracranially implanted with $1 \times 10^5$ tumor cells, then injected at the same coordinates 7 days later with $2 \times 10^6$ plaque-forming units (PFU) of virus, and tumor tissue was analyzed at the indicated time points (Figure 2). Viral load within the tumor was assessed by qPCR 1 h following HSV delivery to confirm initial oHSV input and again 3 and 8 days post injection to assess viral replication kinetics. At 1 h, there was no significant difference in the amounts of KG4:T124 and rQNestin34.5v1 isolated from CT2A tumors, but at 3 and 8 days following oHSV injection, rQNestin34.5v1-treated animals had a significantly greater viral burden compared to KG4:T124-treated animals (Figure 2A). However, no increase in viral load over input was observed with either virus. As an independent measure of virus growth at similar time points, we assessed expression of the viral protein ICP4 in tumor thin sections by immunofluorescence. Early after infection (2 days), the number of infected foci identified in 10 random fields was relatively similar between the two vectors, although rQNestin34.5v1 showed a slightly larger number of infected foci than KG4:T124 (Figure 2B). At later times, the number of rQNestin34.5v1-infected foci decreased, but a more dramatic decrease was seen in the number of KG4:T124-infected foci (see Figure S2A for representative images). We also analyzed *in vivo* HSV replication kinetics using the GL261N4 model. Both our qPCR and immunofluorescence analyses indicated that GL261N4 tumors allowed for prolonged viral presence for both KG4:T124 and rQNestin34.5v1 (Figures 2C and 2D).

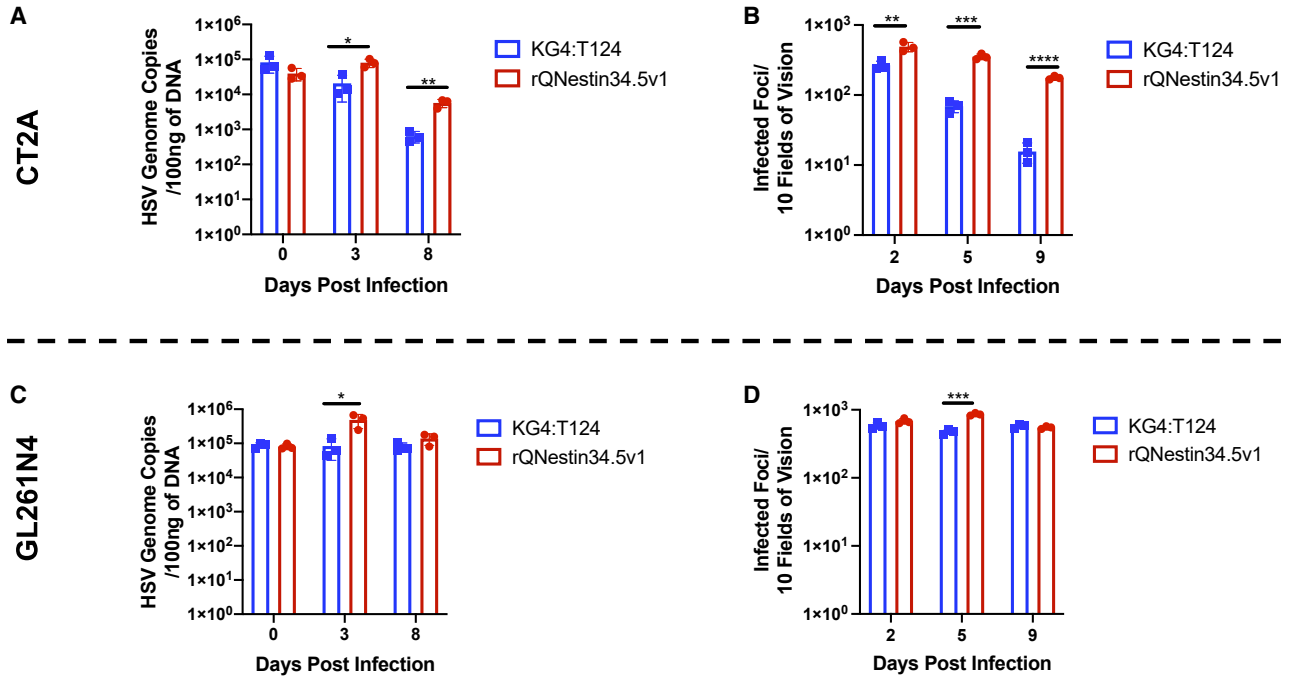


**Figure 2. *In vivo* replication kinetics of KG4:T124 and rQNestin34.5v1 in murine syngeneic gliomas**

HSV genome copies were quantified using qPCR (A and C). Total DNA was isolated per infected condition, and data are displayed as genome copies/100 ng total DNA. In separate experiments, infectious foci were counted per 10 random fields of vision (B and D). Data are representative of the mean ± standard deviation of one experiment per model with 3 animals per treatment group at each indicated time point. Statistical significance was determined by Student's t test. *$p < 0.05$, **$p < 0.01$, ***$p < 0.001$, ****$p < 0.0001$.

Although rQNestin34.5v1 had a somewhat larger viral burden than KG4:T124 early during the infection process, over time no apparent differences in intratumoral viral burden could be seen between vectors (representative images can be found in Figure S2B). Our data indicate that both rQNestin34.5v1 and KG4:T124 survive more efficiently in the GL261N4 model *in vivo* than in CT2A, and rQNestin34.5v1 generally shows increased viral burden compared to KG4:T124 both *in vitro* and *in vivo*.

### Immunological changes induced by oHSV treatment

Based on the viral load analyses above, we chose to analyze intratumoral immune cell accumulation in the two tumor models at 2 and 7 days after treatment. At the 2-day time point, we expected to see the impact of active vector replication on innate immune responses in the tumor microenvironment (TME), while at day 7 adaptive immune responses might be revealed. Evaluation of immune cell recruitment to the CT2A tumor 2 and 7 days post oHSV treatment revealed that HSV therapy did not enhance the total number of live immune cells ($CD45^+$) at either time point. However, 7 days post infection there were 10-fold more immune cells present within the tumor compared to the 2-day time point for each treatment group (Figures 3A and 3H). Analysis of the $CD45^+$ population indicated that the majority of these cells were of myeloid origin ($CD11b^+$, ~70%), and their frequency was not altered between time points or treatment groups (Figures 3B and 3I). Phenotypic analysis of this population revealed differences between oHSV- and PBS-treated tumors at day 2 (Figures 3C–3F), but by day 7 the myeloid population in the CT2A reverted to a vehicle control-treated phenotype (Figures 3J–3M), perhaps due to poor virus growth. At 2 days post treatment the CT2A TME contained a large fraction of $CD45^+$, $CD11b^+$, $Ly6C^+$, $F4/80^-$ immature myeloid cells (Figure 3C), but oHSV therapy did not alter the abundance of these cells. In contrast, the $CD45^+$, $CD11b^+$, $Ly6C^+$, $F4/80^+$ macrophage population was significantly increased by treatment with either KG4:T124 or rQNestin34.5v1 (Figure 3D) compared with PBS controls. We also observed a large influx of granulocytic myeloid cells ($CD45^+$, $CD11b^+$, $Ly6G^+$, $Ly6C^+$, $F4/80^-$) following treatment with KG4:T124 (~8%) or rQNestin34.5 (~20%) compared to PBS-treated controls (~1%) (Figure 3E). Further interrogation of the myeloid fraction revealed that $CD45^{lo}$, $CD11b^+$, $Ly6C^-$ cells, classically characterized as microglia,[20,21] were more abundant in PBS control-treated animals than in animals treated with either virus early after infection (Figure 3F). Figures 3G and 3N summarize the differences between treatment groups in the myeloid compartment of CT2A tumors.

Analysis of the GL261N4 TME at 2 and 7 days post oHSV treatment revealed that oHSV therapy induced similar changes in the myeloid cell population as in the CT2A model at the 2-day but not at the 7-day time point. In the GL261N4 model, oHSV therapy did not enhance the total number of live immune cells ($CD45^+$) at either time point compared to PBS-treated controls, and again at 7 days post infection there were 10-fold more immune cells present within

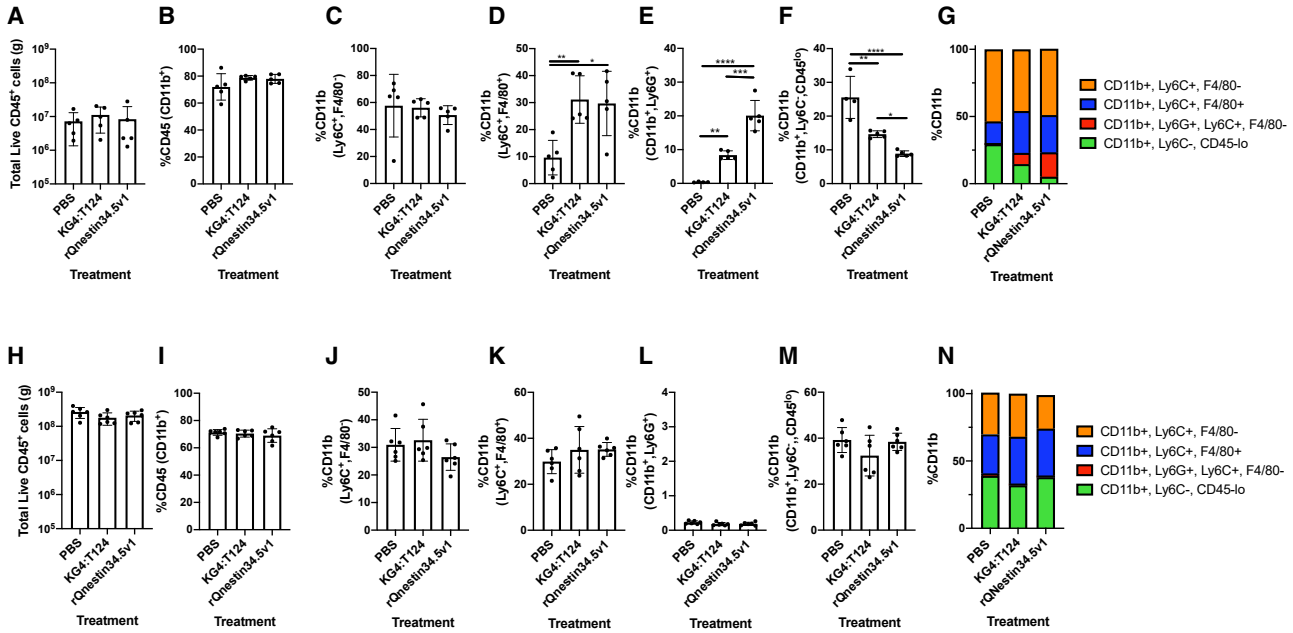


**Figure 3. Immune response to oHSV therapy in the CT2A glioma model**

Tumor microenvironment immunotyping was accomplished via flow cytometry 2 (A–G) and 7 (H–N) days following oHSV infection. Whole-tumor homogenates were used for analysis. The number of total live CD45$^+$ cells analyzed from CT2A tumors was determined as described in Materials and methods (A and H). Myeloid cell (CD45$^+$, CD11b$^+$) frequency was analyzed in the CT2A syngeneic glioma model following KG4:T124 or rQNestin34.5v1 treatment (B and I). Phenotypic interrogation of the respective TME myeloid components was accomplished by flow cytometry (C–G, J, and K). Cell surface markers used to identify each indicated population are detailed on the y axis of each panel. The gating strategy used to identify myeloid cells can be found in Figure S4. Presented data represent the mean ± standard deviation from one experiment which is representative of two experimental replicates, with 5–6 animals per treatment group. Statistical significance was determined by one-way ANOVA with Tukey's multiple comparisons of means. *$p < 0.05$, **$p < 0.01$, ***$p < 0.001$, ****$p < 0.0001$.

the tumor than at day 2 (Figures 4A and 4H). Myeloid abundance was not changed 2 days post oHSV treatment, but 7 days post KG4:T124 or rQNestin34.5v1 administration, the myeloid cell fraction was significantly (****$p < 0.0001$) less abundant than in vehicle control-treated animals (Figures 4B and 4I). At 2 days post oHSV therapy, the CD45$^+$, CD11b$^+$, Ly6C$^+$, F4/80$^-$ myeloid cells were significantly (*$p < 0.05$) increased compared to vehicle-treated animals, but this population mirrored that of PBS control-treated animals 7 days post oHSV treatment (Figures 4C and 4J). Interestingly, the CD45$^+$, CD11b$^+$, Ly6C$^+$, F4/80$^+$ macrophage population was significantly increased by treatment with either KG4:T124 or rQNestin34.5v1 at both 2 and 7 days following therapy (Figures 4D and 4K), but only rQNestin34.5v1 induced a statistically significant (**$p < 0.01$) accumulation of these cells 7 days post infection (Figure 4K). As seen in the CT2A model, virus treatment induced the recruitment of granulocytic myeloid cells (CD45$^+$, CD11b$^+$, Ly6G$^+$, Ly6C$^+$, F4/80$^-$) 2 days post treatment compared to vehicle-treated control animals, and this population was almost undetectable 7 days post infection (Figures 4E and 4L). Unlike what was observed in the CT2A model, CD45$^{lo}$, CD11b$^+$, Ly6C$^-$ microglia remained significantly increased in PBS-treated animals compared to oHSV-treated animals 7 days post therapy (Figures 4F and 4M). Overall, oHSV induced changes mainly in macrophage abundance of GL261N4 tumors at both 2 and 7 days post treatment (Figures 4G and 4N). Together, these analyses demonstrated a profound difference in the response of the two tumor types to oHSV treatment.

We also analyzed the recruitment of natural killer (NK) cells, CD8$^+$, and CD4$^+$ T cells in both models at both time points. Treatment of CT2A or GL261N4 tumors with rQNestin34.5v1 or KG4:T124 did not enhance the recruitment of any of these cell types at 2 days post infection compared with PBS-treated tumors (Figures S4A–S4F), and overall, the three populations were scarce in both models at 2 days. This phenotype was also observed in the CT2A model at 7 days post treatment (Figures 5A–5C). However, in the GL261N4 model, HSV altered the abundance of all three cell types at 7 days, reducing NK cell recruitment compared to PBS (Figure 5H), while inducing a significant accumulation of CD8$^+$ and CD4$^+$ T cells (Figures 5I and 5J).

We interrogated the activation status of the CD8$^+$ and CD4$^+$ T cells at 7 days post treatment, assessing cellular expression of the classical activation marker CD69[22] and the activation/exhaustion marker PD-1.[23] In the GL261N4 model, HSV treatment enhanced PD-1 expression on both CD8$^+$ and CD4$^+$ T cells (Figures 5K and 5M) without changing the abundance of CD69$^+$-expressing CD8$^+$ or CD4$^+$ T cells (Figures 5L and 5N). However, in the CT2A model, neither KG4:T124 nor rQNestin34.5v1 altered PD-1 or CD69 expression on CD8$^+$ or CD4$^+$ T cells (Figures 5D–5G). Overall, the CD69$^+$

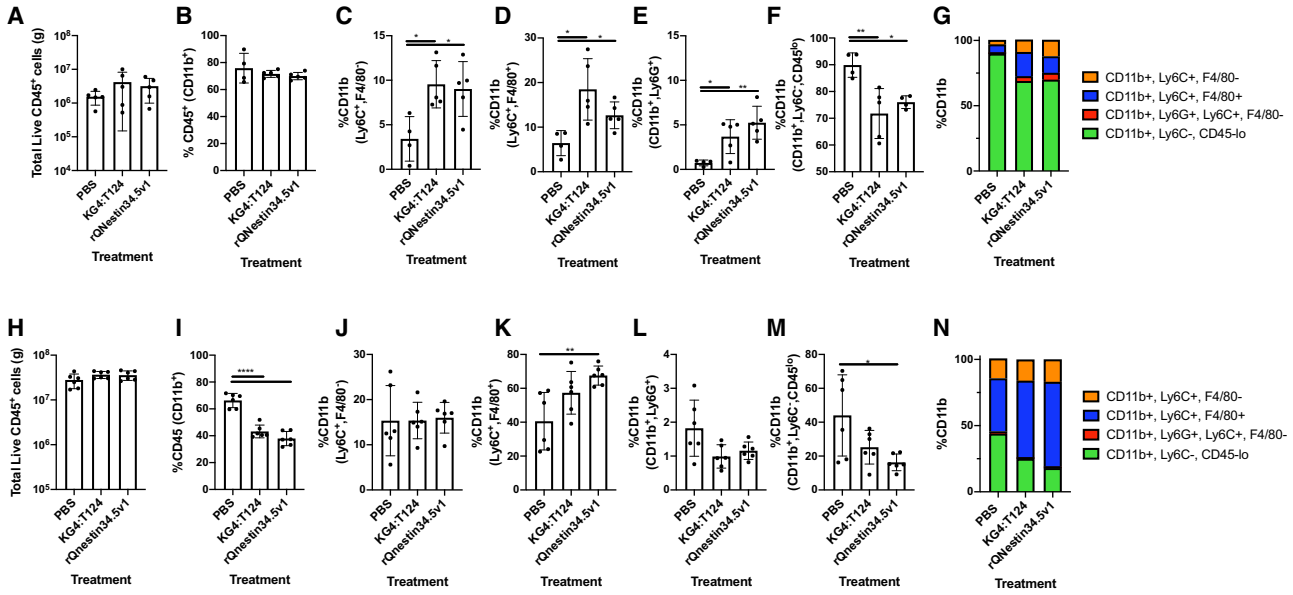


**Figure 4. Immune response to oHSV therapy in the GL261N4 glioma model**

Tumor microenvironment immunotyping was accomplished via flow cytometry 2 (A–G) and 7 (H–N) days following oHSV infection. Whole-tumor homogenates were used for analysis. The number of total live CD45$^+$ cells analyzed from GL261N4 was determined as described in the Materials and methods (A and H). Myeloid cell (CD45$^+$, CD11b$^+$) frequency was analyzed in GL261N4 syngeneic gliomas following oHSV treatment (B and I). Phenotypic interrogation of the respective TME myeloid compartments was accomplished by flow cytometry (C–G, J, and K). Cell surface markers used to identify each indicated population are detailed on the y axis of each panel. The gating strategy used to identify myeloid cells can be found in Figure S4. Presented data represent the mean ± standard deviation from one experiment which is representative of two experimental replicates, with 4–5 animals per treatment group. Statistical significance was determined by one-way ANOVA with Tukey's multiple comparisons of means. *$p < 0.05$, **$p < 0.01$, ****$p < 0.0001$.

fraction of T cells in CT2A tumors was smaller than in GL261N4 tumors, while the PD-1$^+$ fraction was larger in CT2A than in GL261N4 tumors. Our immunological analyses indicate that recruitment of immune cells to the tumor following oHSV therapy appears to associate with length of virus persistence in the tumor.

### Therapeutic efficacy of oHSV treatment using murine syngeneic glioma models

The observation that the GL261N4 model was amenable to sustaining oHSV within the tumor and the fact that macrophages and T cells were recruited to these tumors led us to question whether oHSV would be able to limit GL261N4 tumor progression. Using magnetic resonance imaging (MRI), we determined the ability of rQNestin34.5v1 and KG4:T124 to limit GL261N4 tumor progression. Experimental conditions are outlined in Figure 6A. Representative images of two animals per treatment group prior to HSV treatment and 7 days following therapy are displayed in Figure 6B. We quantified tumor volume before HSV therapy and 7 days following, as described in Materials and methods. Prior to HSV therapy, there was no significant difference in the tumor volume between any of the animals (Figure 6C). However, following HSV therapy, rQNestin34.5v1-treated animals had significantly smaller tumors than animals treated with either PBS or KG4:T124 (Figure 6C) and a correspondingly smaller change in tumor volume relative to pre-treatment. Despite the inability of KG4:T124 to limit tumor progression, both vectors protected animals from losing weight compared to PBS-treated animals (Figure 6D). These results were consistent with *in vitro* and *in vivo* vector growth kinetics and macrophage recruitment.

Finally, we asked whether oHSV treatment would provide a therapeutic benefit in either the CT2A or GL261N4 model following intratumoral vector delivery. The results showed that neither KG4:T124 nor rQNestin34.5v1 provided a survival benefit for animals engrafted with CT2A tumors. In contrast, rQNestin34.5v1 was found to induce an increase, albeit limited, in the survival of GL261N4 tumor-bearing animals (Figures 7A and 7B).

## DISCUSSION

Clinical evaluation of oncolytic virus therapies for the treatment of a variety of human cancers is becoming commonplace. In 2019, 118 clinical trials implementing oncolytic viruses to treat cancer were underway.[24] Oncolytic viruses are an attractive anti-cancer therapy, as they are able to destroy infected tumor cells, regardless of the cell's chemo- or radiation-resistance status, while priming anti-tumor immune responses.[25,26] A plethora of virus species are being used as oncolytic viruses (e.g., adeno, vaccinia, polio, measles), but oHSV became the frontrunner with the FDA approval of T-VEC (Imlygic) for the treatment of melanoma.[6] Moreover, several clinical trials are currently underway or are actively recruiting to assess oHSV therapies for glioblastoma (UK0033, UK0136, NCT02457845, NCT02062827, NCT

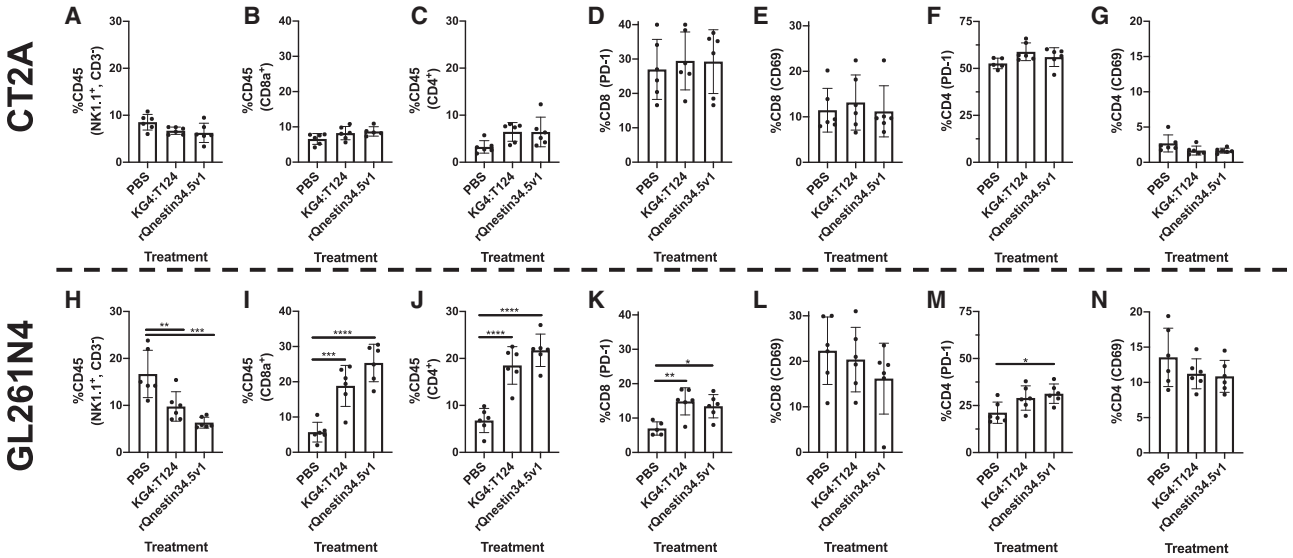


**Figure 5. Analysis of NK cell and T cell responses 7 days post oHSV treatment**

Flow cytometry was used to analyze natural killer, $CD8^+$, and $CD4^+$ T cell recruitment to the tumor following oHSV treatment of CT2A or GL261N4 7 days post infection (A–C and H–J). PD-1 expression on T cells isolated form either tumor was further interrogated (D, F, K, and M). CD69 expression was also analyzed on $CD8^+$ and $CD4^+$ T cells (E, G, L, and N). Data represent the mean ± standard deviation of one of two experiments per model with 5–6 animals per group. Statistical significance was determined by one-way ANOVA with Tukey's multiple comparisons of means. *$p < 0.05$, **$p < 0.01$, ***$p < 0.001$, ****$p < 0.0001$.

03152318, and UMIN000002661).[27] These trials have been largely justified based on observations from pre-clinical animal models using human xenograft tissue in immunodeficient animals. In these studies, oHSV replicated well in the tumors and provided significant survival benefit with a single dose of oHSV.[28–30] Unfortunately, early-phase results indicate that only a small subset of GBM patients respond to oHSV therapy, and little evidence to support the utility of oHSV to prevent recurrent disease has been forthcoming.[24] Barriers potentially limiting oHSV efficacy include the length and magnitude of viral replication *in vivo* and the immunosuppressive TME, further limiting oHSV efficacy. Here we sought to analyze the impact of oHSV replication on animal survival and recruitment of immunologically active cells into the TME using syngeneic GBM models in immune-competent mice. These studies involved two oncolytic HSV vectors, KG4:T124 and rQNestin34.5v1, which are early-generation derivatives of oHSV vectors that are being used in patient trials; we assessed their ability to treat two syngeneic tumor models, CT2A and GL261N4, which represent differences in pathogenesis and antigenicity.[17] Our findings confirm the importance of prolonged vector presence within the tumor and the need for enhanced methods to induce anti-tumor immunity.

Our initial studies focused on comparing viral replication of both oHSV vectors in murine gliomas *in vitro*. We determined that rQNestin34.5v1 replicated more efficiently *in vitro* than KG4:T124. Next, we evaluated oHSV replication kinetics *in vivo*. Unlike our *in vitro* experiments, where we observed no differences in replication capacity for either virus between cell lines (Figure S1B), viral presence in the CT2A model for both vectors was short-lived, while GL261N4 allowed for prolonged virus presence. However, in both models, rQNestin34.5v1 had a significantly larger viral burden compared to KG4:T124, aligning with our *in vitro* observations. The mechanism underlying poor virus growth in CT2A tumors is unknown but may be related to rapid tumor cell growth combined with reduced permissivity. However, *in vitro* studies indicate that virus attachment/penetration is not the reason, since both viruses infected cells with similar efficiency (Figure S1A).

Shortly after vector administration (2 days post infection) in CT2A and GL261N4 tumors, virus treatment induced an influx of granulocytes and macrophages, while an accumulation of $CD45^+$, $CD11b^+$, $Ly6C^+$, $F4/80^-$ immature myeloid cells was only observed in oHSV-treated GL261N4 tumors; CT2A tumors contained high levels of the latter cells regardless of treatment. $CD45^+$, $CD11b^+$, $Ly6C^+$, $F4/80^-$ cells are typically considered monocytic-myeloid-derived suppressor cells (MDSC) that are immunosuppressive and known to limit productive anti-tumor immune responses[31,32] and oHSV replication.[33] The high abundance of these cells within the CT2A TME could explain the minimal oHSV replication in this model and why animals bearing CT2A tumors were impervious to treatment with either virus. While oHSV induced otherwise similar changes in both models early after oHSV administration, at 7 days, when only GL261N4 tumors contained readily detectable viral loads, the CT2A TME had reverted to a control-treated phenotype, whereas GL261N4 tumors remained significantly different in immune cell makeup compared to PBS-treated animals. At the later time point, both vectors induced similar changes in immune cell recruitment, but only rQNestin34.5v1 treatment continued to support statistically significant increased macrophage accumulation. As macrophages are

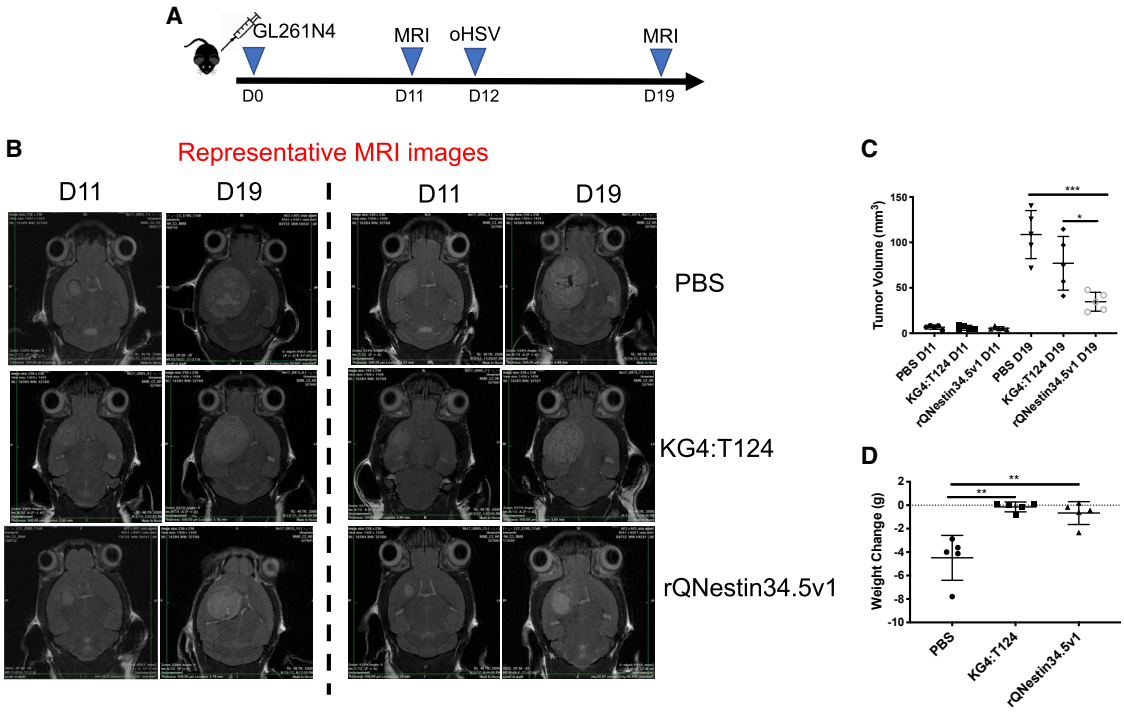


**Figure 6. rQNestin34.5v1 and KG4T:124 impact on GL261N4 tumor progression**

Experimental design schematic (A). Representative MRI images of mice bearing GL261N4 tumors (B). Animals were imaged on day 11, treated on day 12 following tumor implant with rQNestin34.5v1 or KG4:T124, and reimaged on day 19. Images are representative of two animals per treatment group. Tumor volume was determined as described in Materials and methods (C). Evaluation of animal weight loss 7 days following oHSV treatment (D). Data represent the mean ± standard deviation of one experiment with 5 animals per treatment group. Statistical significance was determined by one-way ANOVA with Tukey's multiple comparisons of means. *$p < 0.05$, **$p < 0.01$, ***$p < 0.001$.

pivotal to limiting GBM progression and needed to induce productive anti-tumor immunity,[34,35] the enhanced responses following rQNestin34.5v1 treatment could explain why a few animals bearing GL261N4 tumors treated with rQNestin34.5v1 survived long term. Importantly, both oHSV vectors analyzed induced $CD8^+$ and $CD4^+$ T cell recruitment 7 days post oHSV treatment, but a significant portion of these cells were $PD\text{-}1^+$, and neither vector was able to enhance T cell activation (CD69 expression) compared to control-treated animals. This observation is consistent with previous studies; treatment of GBM with an oHSV expressing IL-12 significantly enhanced animal survival, and CD69 expression was not increased compared to mock-treated animals, suggesting the possibility that CD69 is not essential for T cell activation in the context of GBM.[35] These data indicate that prolonged oHSV presence can enhance adaptive immune cell recruitment to the tumor but is insufficient to inspire T cell activation. Moreover, the diminutive virus presence within CT2A tumors and proclivity of these tumors to revert to an untreated tumor phenotype following oHSV treatment help to explain previous reports indicating that rQNestin34.5v1 was unable to limit CT2A tumor progression compared to vehicle control-treated animals,[18] a phenotype not observed in the GL261N4 model (Figure 6).

Overall, we conclude that strain differences and methods for vector attenuation may likely impact vector performance and oncolytic activity in the context of mouse GBM. Of the two strains tested, the KOS strain is considered less pathogenic compared to the F strain and other HSV-1 strains,[36] but both vectors in this study retain neurovirulence genes, in particular ICP34.5, which is deleted in the majority of other oHSVs.[8] However, regardless of oHSV strain or means of attenuation, the two oHSV tested here induced similar immune cell recruitment to the tumor mass, and the duration of the immune response correlated with the duration of oHSV presence within the tumor. Moving forward, oHSV therapy will likely require the use of vectors capable of expressing a combination of immunomodulatory gene products designed to enhance the recruitment and activity of specific immune cells, such as macrophages and cytotoxic T cells.

## MATERIALS AND METHODS

### Cell lines, viruses, and animals

CT2A and GL261N4 cells have been previously described.[16] Cells were grown in DMEM (Corning) supplemented with 1% penicillin/streptomycin and 10% fetal bovine serum (FBS) (Sigma). The HSV-1 KOS strain derivative KG4:T124 has been previously described.[13] We have also inserted a gateway cassette in between UL3 and UL4 to allow for rapid immunotherapeutic gene insertion. The HSV-F-strain derivative rQNestin34.5 has been previously described.[9] Viruses were grown on Vero cells (ATCC) and titered using Vero cells. Functional titers for tumor cell lines were not determined; all

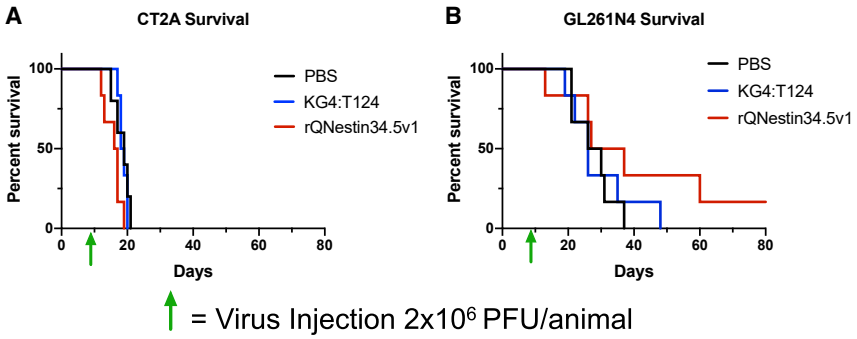


**Figure 7. oHSV therapeutic benefit in the CT2A and GL261N4 syngeneic mouse GBM models**

Survival of animals bearing CT2A (A) or Gl261N4 (B) brain tumors treated with rQNestin34.5v1 or KG4:T124 compared to PBS control-treated mice. Green arrows indicate the day on which a dose of $2 \times 10^6$ PFU/animal was administered (day 7). Data are representative of two experiments with 6 animals per treatment group. Statistical significance was determined by log-ranked (Mantel-Cox) test. There was no statistical difference between treatment groups.

multiplicities of infection (MOI) for *in vitro* experiments were based on Vero titers and do not reflect cell-type-specific differences in entry and plaquing. Female C57BL/6 wild-type (WT) mice were obtained from The Jackson Laboratory. Animals were maintained in the Animal Facility at the University of Pittsburgh (Pittsburgh, PA, USA) per an Institutional Animal Care and Use Committee-approved protocol. For tumor implantation, anesthetized mice were fixed in a stereotactic apparatus, a burr hole was drilled 2 mm lateral and 0.5 mm anterior to the bregma to a depth of 3 mm, and $2 \times 10^5$ of either CT2A or GL261N4 cells in 2 μL PBS were implanted. At 7 days post tumor cell implant, the mice were anesthetized again and stereotactically inoculated at the same coordinates with 3 μL PBS or virus ($2 \times 10^6$ PFU). Animals were observed daily and euthanized at the indicated time points or when showing signs of morbidity.

### Viral entry assay

Indicated cell types were plated at 70%–80% confluency in twelve-well tissue-culture-treated dishes. The following day, cells were infected with a MOI of three. One and a half hours following infection, viral input was removed with a 20% glycine solution diluted in PBS. Six hours following infection, medium was removed and cells trypsinized. Cells were fixed with 4% paraformaldehyde (PFA) (Fisher Scientific) for 30 min at room temperature, then washed with PBS. Cells were then permeabilized with a 0.1% Triton X-100 (Sigma) solution for 10 min at room temperature and washed with PBS. Cells were then incubated in a 10% horse serum solution diluted in PBS for 1 h at room temperature. Following, cells were incubated with the anti-ICP4 primary antibody (Santa Cruz) overnight at 4°C. Cells were washed with PBS then incubated with the secondary anti-mouse Alexa 488 conjugated antibody (Fisher Scientific) for 1 h at room temperature in the dark. Cells were washed with PBS, and data were collected using a BD Accuri c6 Plus. Data were analyzed using FlowJo version 10.3.

### Viral growth assay

Indicated cell types were plated at 70%–80% confluency in twelve-well tissue-culture-treated dishes. The following day, cells were infected with either a MOI of 0.1 or 1. One and a half hours following infection, viral input was removed with a 10%–20% glycine solution, depending on the cell type. Cells and supernatants were harvested at indicated time points, combined, and sonicated three times using 20-s intervals. Cell debris was removed by centrifugation, and samples were stored at −80°C. Viral supernatants were titered using Vero cells. Supernatants were serially diluted in serum-free media and plated on 80%–90% confluent Vero monolayers. One and a half hours after infection, cells were overlaid with a 1% carboxymethyl cellulose, 10% serum, 1% penicillin/streptomycin, DMEM solution. Three days following infection, viral plaques were counted using an inverted fluorescent microscope.

### Viral mediated cytolysis

Indicated cell types were plated at 70%–80% confluency in twelve-well tissue-culture-treated dishes. The following day, cells were infected with a MOI of 0.1 for human cells or 1 for murine cells. Seventy-two hours after infection, an alamarBLUE assay (Thermo Fisher) was conducted. Briefly, alamar blue reagent was diluted 10-fold directly into infected cell wells. Supernatant was monitored for color change, and upon color change absorbance was measured (540/560) using a Biotek synergy 4 plate reader and analyzed with Gen5 software.

### Flow cytometry

Single-cell suspensions of brain tumors were generated by gentle mechanical disassociation followed by enzymatic disassociation. The enzymatic solution (EZ) is as follows: 32 mg collagenase IV (Worthington), 10 mg deoxyribonuclease I (Worthington), 20 mg soybean trypsin inhibitor (Worthington), resuspended in 10 mL of PBS. Enzymatic disassociation took place in 500 μL of EZ for 30 min shaking at 37°C. Following disassociation, cells were passed through a 70 μM filter (Fisher), then washed with PBS. Cells were then stained with fluorescently conjugated antibodies for flow cytometry. Antibodies used include: Near IR LIVE/DEAD (Thermo Scientific); CD45 (30-F11), LY6C (HK1.4), CD8 (53-6.7), CD4 (GK1.5), CD11c (N418), NK1.1 (PK136), CD38 (90), CD103 (2E7), and CD279 (29F.1A12) (Biolegend); and CD11b (M1/70), LY6G (1A8), CD3 (17A2), and CD4 (RM4-5) (BD Biosciences). Total cell counts were determined using CountBright Absolute Counting Beads (Invitrogen). Data were collected using either a BD LSRII or a BD Accuri c6 Plus. Data were analyzed using FlowJo version 10.3.

### *In vivo* MRI analysis

Mice received general inhalation anesthesia with isoflurane for *in vivo* brain imaging. Depth of anesthesia was monitored by toe reflex

(extension of limbs, spine positioning) and respiration rate. Once the plane of anesthesia was established, it was maintained with 1%–2% isoflurane in oxygen via a designated nose cone, and the mouse was transferred to the designated animal bed for imaging. Respiration was monitored using a pneumatic sensor placed between the animal bed and the mouse's abdomen, while rectal temperature was measured with a fiber optic sensor and the core temperature maintained at 36.8°C + 0.2°C with a feedback-controlled warm air source (SA Instruments, Stony Brook, NY, USA). *In vivo* brain MRI was carried out on a Bruker BioSpec 70/30 USR spectrometer (Bruker BioSpin MRI, Billerica, MA, USA) operating at 7-T field strength, equipped with an actively shielded gradient system B-GA12S2 gradient with 440 mT/m gradient strength and slew rate 3440 T/m/s as well as a quadrature radio-frequency volume coil with an inner diameter of 35 mm. Multi-planar $T_2$-weighted anatomical imaging covering the whole brain volume was acquired with rapid imaging with refocused echoes (RARE) pulse sequence with the following parameters: field of view (FOV) = 2 cm, matrix = 256 × 256, slice thickness = 0.6 mm, in-plane resolution = 78 μm × 78 μm, RARE factor = 8, echo time (TE) = 12 ms, effective echo time (ETE) = 48 ms, repetition time (TR) = 1,600 ms, flip angle (FA) = 180°. The multi-planar $T_2$-weighted RARE images were exported to DICOM format and analyzed by blinded independent observers using the open source ITK-SNAP (http://www.itksnap.org/pmwiki/pmwiki.php) brain segmentation software. The tumor volume is defined as areas with hyperintensity on the $T_2$-weighted RARE images. The hemorrhage volume is defined as areas with hypointensity on the $T_2$-weighted RARE images.

#### Sequencing and genome assembly

We performed whole-genome sequencing on both KG4:T124 and rQNestin34.5v1 to ensure there were no unexpected mutations; none were found (data not shown). Sequencing took place as previously described.[37] All sequencing was performed by the University of Pittsburgh's Health Sciences Sequencing core. Briefly, purified viral DNA was harvested from purified virions using a DNA blood and tissue extraction kit (QIAGEN). The sequencing was designed to ensure a 40× genome coverage. Illumina sequencing reads (150 × 150 paired-end sequencing reads) were mapped to the parental *in silico*-derived sequences KG4:T124-GW or rQNestin34.5v1 using the CLC genomic work bench. All resequencing data are available from authors upon request.

#### *In vivo* growth kinetics

Genome copy number was determined as previous described.[38] Briefly, the entire infected tumor-bearing brain hemisphere was harvested. Total DNA was extracted using the QIAGEN DNA blood and tissue extraction kit. gc titers were calculated relative to a standard curve generated for each experiment using a 10-fold dilution series of plasmid pUL5 (corresponding to $3 \times 10^6$ to $3 \times 10^2$ copies of the HSV genome) and a custom FAM-MGB TaqMan primer probe set (UL5qPCR-F, UL5qPCR-R, UL5 MGB probe; Thermo Fisher Scientific). *In vivo* immunofluorescence was performed by snap freezing infected tumor-bearing brain hemispheres in OTC (Tissuetek) freezing compound using liquid nitrogen. 12 μm sections were produced using a Cryostat Microm HM5050E. Permeabilized sections were stained for 48 h with anti-ICP4 primary antibody (Santa Cruz) and anti-nestin primary antibody (Santa Cruz). Alexa 488 and Alexa 594 conjugated secondary antibodies (Molecular Probes) were incubated for an hour at room temperature. DAPI staining took place for 10 min at room temperature. Images were captured using Nikon Diaphot fluorescence microscope (Nikon, Melville, NY, USA) and MetaMorph imaging software (Molecular Devices, San Jose, CA, USA).

#### Statistical analysis

GraphPad Prism 8 software was used for all statistical analyses. Averages for each experiment are shown ± SD. As noted in the relevant figure legends, unpaired Student's t tests or one-way or two-way ANOVAs were performed.

## SUPPLEMENTAL INFORMATION

Supplemental information can be found online at https://doi.org/10.1016/j.omto.2021.07.009.

## ACKNOWLEDGMENTS

This work was supported by grants from the NIH (R01 CA222804 to J.C.G.; P01 CA163205 to J.C.G., W.F.G., and E.A.C.; and T32 CA082084 to J.W.J).

## AUTHOR CONTRIBUTIONS

Conceptualization, J.W.J., B.L.H., J.B.C., and J.C.G.; Methodology, J.W.J., M.M., E.A.C., G.K., J.B.C., and J.C.G.; Investigation, J.W.J., B.L.H., V.K.S., and L.B.; Writing – original draft, J.W.J.; Writing – review & editing, J.W.J., B.L.H., V.K.S., E.A.C., W.F.G., G.K., J.B.C., and J.C.G.; Funding acquisition, J.W.J., E.A.C., and J.C.G.; Resources, M.M. and W.F.G.; Supervision, W.F.G., J.B.C., and J.C.G.

## DECLARATION OF INTERESTS

J.C.G. is an inventor of intellectual property licensed to Coda Biotherapeutics, Inc. (San Francisco, CA). J.B.C. and J.C.G. are inventors of intellectual property licensed to Oncorus, Inc. (Cambridge, MA, USA). J.C.G. is a consultant and member of the Scientific Advisory Boards of Coda Biotherapeutics, Inc. and Oncorus, Inc. W.F.G. is a consultant of Oncorus, Inc. E.A.C. holds ownership interest (including patents) in DNAtrix and is a consultant/advisory board member for Advantagene, DNAtrix, and NanoTherapeutics. The remaining authors declare no competing interests.

## REFERENCES

1. Ostrom, Q.T., Gittleman, H., Truitt, G., Boscia, A., Kruchko, C., and Barnholtz-Sloan, J.S. (2018). CBTRUS Statistical Report: Primary Brain and Other Central Nervous System Tumors Diagnosed in the United States in 2011-2015. Neuro-oncol. *20* (suppl_4), iv1–iv86.

2. Weller, M., Wick, W., Aldape, K., Brada, M., Berger, M., Pfister, S.M., Nishikawa, R., Rosenthal, M., Wen, P.Y., Stupp, R., and Reifenberger, G. (2015). Glioma. Nat. Rev. Dis. Primers *1*, 15017.

3. Koshy, M., Villano, J.L., Dolecek, T.A., Howard, A., Mahmood, U., Chmura, S.J., Weichselbaum, R.R., and McCarthy, B.J. (2012). Improved survival time trends for

glioblastoma using the SEER 17 population-based registries. J. Neurooncol. *107*, 207–212.

4. Stupp, R., Hegi, M.E., Mason, W.P., van den Bent, M.J., Taphoorn, M.J., Janzer, R.C., Ludwin, S.K., Allgeier, A., Fisher, B., Belanger, K., et al.; European Organisation for Research and Treatment of Cancer Brain Tumour and Radiation Oncology Groups; National Cancer Institute of Canada Clinical Trials Group (2009). Effects of radiotherapy with concomitant and adjuvant temozolomide versus radiotherapy alone on survival in glioblastoma in a randomised phase III study: 5-year analysis of the EORTC-NCIC trial. Lancet Oncol. *10*, 459–466.
5. Tamimi, A.F., and Juweid, M. (2017). Epidemiology and Outcome of Glioblastoma. In Glioblastoma, S. De Vleeschouwer, ed. (Codon Publications).
6. Andtbacka, R.H., Kaufman, H.L., Collichio, F., Amatruda, T., Senzer, N., Chesney, J., Delman, K.A., Spitler, L.E., Puzanov, I., Agarwala, S.S., et al. (2015). Talimogene Laherparepvec Improves Durable Response Rate in Patients With Advanced Melanoma. J. Clin. Oncol. *33*, 2780–2788.
7. Markert, J.M., Medlock, M.D., Rabkin, S.D., Gillespie, G.Y., Todo, T., Hunter, W.D., Palmer, C.A., Feigenbaum, F., Tornatore, C., Tufaro, F., and Martuza, R.L. (2000). Conditionally replicating herpes simplex virus mutant, G207 for the treatment of malignant glioma: results of a phase I trial. Gene Ther. *7*, 867–874.
8. Bommareddy, P.K., Peters, C., Saha, D., Rabkin, S.D., and Kaufman, H.L. (2018). Oncolytic Herpes Simplex Viruses as a Paradigm for the Treatment of Cancer. Annu. Rev. Cancer Biol. *2*, 155–173.
9. Kambara, H., Okano, H., Chiocca, E.A., and Saeki, Y. (2005). An oncolytic HSV-1 mutant expressing ICP34.5 under control of a nestin promoter increases survival of animals even when symptomatic from a brain tumor. Cancer Res. *65*, 2832–2839.
10. Ishiwata, T., Matsuda, Y., and Naito, Z. (2011). Nestin in gastrointestinal and other cancers: effects on cells and tumor angiogenesis. World J. Gastroenterol. *17*, 409–418.
11. Chou, J., Kern, E.R., Whitley, R.J., and Roizman, B. (1990). Mapping of herpes simplex virus-1 neurovirulence to gamma 134.5, a gene nonessential for growth in culture. Science *250*, 1262–1266.
12. Chiocca, E.A., Nakashima, H., Kasai, K., Fernandez, S.A., and Oglesbee, M. (2020). Preclinical Toxicology of rQNestin34.5v.2: An Oncolytic Herpes Virus with Transcriptional Regulation of the ICP34.5 Neurovirulence Gene. Mol. Ther. Methods Clin. Dev. *17*, 871–893.
13. Mazzacurati, L., Marzulli, M., Reinhart, B., Miyagawa, Y., Uchida, H., Goins, W.F., Li, A., Kaur, B., Caligiuri, M., Cripe, T., et al. (2015). Use of miRNA response sequences to block off-target replication and increase the safety of an unattenuated, glioblastoma-targeted oncolytic HSV. Mol. Ther. *23*, 99–107.
14. Silber, J., Lim, D.A., Petritsch, C., Persson, A.I., Maunakea, A.K., Yu, M., Vandenberg, S.R., Ginzinger, D.G., James, C.D., Costello, J.F., et al. (2008). miR-124 and miR-137 inhibit proliferation of glioblastoma multiforme cells and induce differentiation of brain tumor stem cells. BMC Med. *6*, 14.
15. Uchida, H., Chan, J., Goins, W.F., Grandi, P., Kumagai, I., Cohen, J.B., and Glorioso, J.C. (2010). A double mutation in glycoprotein gB compensates for ineffective gD-dependent initiation of herpes simplex virus type 1 infection. J. Virol. *84*, 12200–12209.
16. Nakashima, H., Nguyen, T., Kasai, K., Passaro, C., Ito, H., Goins, W.F., Shaikh, I., Erdelyi, R., Nishihara, R., Nakano, I., et al. (2018). Toxicity and Efficacy of a Novel GADD34-expressing Oncolytic HSV-1 for the Treatment of Experimental Glioblastoma. Clin. Cancer Res. *24*, 2574–2584.
17. Oh, T., Fakurnejad, S., Sayegh, E.T., Clark, A.J., Ivan, M.E., Sun, M.Z., Safaee, M., Bloch, O., James, C.D., and Parsa, A.T. (2014). Immunocompetent murine models for the study of glioblastoma immunotherapy. J. Transl. Med. *12*, 107.
18. Alayo, Q.A., Ito, H., Passaro, C., Zdioruk, M., Mahmoud, A.B., Grauwet, K., Zhang, X., Lawler, S.E., Reardon, D.A., Goins, W.F., et al. (2020). Glioblastoma infiltration of both tumor- and virus-antigen specific cytotoxic T cells correlates with experimental virotherapy responses. Sci. Rep. *10*, 5095.
19. Khalsa, J.K., Cheng, N., Keegan, J., Chaudry, A., Driver, J., Bi, W.L., Lederer, J., and Shah, K. (2020). Immune phenotyping of diverse syngeneic murine brain tumors identifies immunologically distinct types. Nat. Commun. *11*, 3912.
20. DePaula-Silva, A.B., Gorbea, C., Doty, D.J., Libbey, J.E., Sanchez, J.M.S., Hanak, T.J., Cazalla, D., and Fujinami, R.S. (2019). Differential transcriptional profiles identify microglial- and macrophage-specific gene markers expressed during virus-induced neuroinflammation. J. Neuroinflammation *16*, 152.
21. Zhang, G.X., Li, J., Ventura, E., and Rostami, A. (2002). Parenchymal microglia of naïve adult C57BL/6J mice express high levels of B7.1, B7.2, and MHC class II. Exp. Mol. Pathol. *73*, 35–45.
22. Cibrián, D., and Sánchez-Madrid, F. (2017). CD69: from activation marker to metabolic gatekeeper. Eur. J. Immunol. *47*, 946–953.
23. Wherry, E.J., and Kurachi, M. (2015). Molecular and cellular insights into T cell exhaustion. Nat. Rev. Immunol. *15*, 486–499.
24. Zheng, M., Huang, J., Tong, A., and Yang, H. (2019). Oncolytic Viruses for Cancer Therapy: Barriers and Recent Advances. Mol. Ther. Oncolytics *15*, 234–247.
25. Zhang, Q., and Liu, F. (2020). Advances and potential pitfalls of oncolytic viruses expressing immunomodulatory transgene therapy for malignant gliomas. Cell Death Dis. *11*, 485.
26. Wennier, S.T., Liu, J., and McFadden, G. (2012). Bugs and drugs: oncolytic virotherapy in combination with chemotherapy. Curr. Pharm. Biotechnol. *13*, 1817–1833.
27. Ning, J., and Wakimoto, H. (2014). Oncolytic herpes simplex virus-based strategies: toward a breakthrough in glioblastoma therapy. Front. Microbiol. *5*, 303.
28. Friedman, G.K., Bernstock, J.D., Chen, D., Nan, L., Moore, B.P., Kelly, V.M., Youngblood, S.L., Langford, C.P., Han, X., Ring, E.K., et al. (2018). Enhanced Sensitivity of Patient-Derived Pediatric High-Grade Brain Tumor Xenografts to Oncolytic HSV-1 Virotherapy Correlates with Nectin-1 Expression. Sci. Rep. *8*, 13930.
29. Ikeda, K., Ichikawa, T., Wakimoto, H., Silver, J.S., Deisboeck, T.S., Finkelstein, D., Harsh, G.R., 4th, Louis, D.N., Bartus, R.T., Hochberg, F.H., and Chiocca, E.A. (1999). Oncolytic virus therapy of multiple tumors in the brain requires suppression of innate and elicited antiviral responses. Nat. Med. *5*, 881–887.
30. Martuza, R.L., Malick, A., Markert, J.M., Ruffner, K.L., and Coen, D.M. (1991). Experimental therapy of human glioma by means of a genetically engineered virus mutant. Science *252*, 854–856.
31. DeCordova, S., Shastri, A., Tsolaki, A.G., Yasmin, H., Klein, L., Singh, S.K., and Kishore, U. (2020). Molecular Heterogeneity and Immunosuppressive Microenvironment in Glioblastoma. Front. Immunol. *11*, 1402.
32. Nduom, E.K., Weller, M., and Heimberger, A.B. (2015). Immunosuppressive mechanisms in glioblastoma. Neuro-oncol. *17* (*Suppl 7*), vii9–vii14.
33. Wojtasiak, M., Pickett, D.L., Tate, M.D., Bedoui, S., Job, E.R., Whitney, P.G., Brooks, A.G., and Reading, P.C. (2010). Gr-1+ cells, but not neutrophils, limit virus replication and lesion development following flank infection of mice with herpes simplex virus type-1. Virology *407*, 143–151.
34. Galarneau, H., Villeneuve, J., Gowing, G., Julien, J.P., and Vallières, L. (2007). Increased glioma growth in mice depleted of macrophages. Cancer Res. *67*, 8874–8881.
35. Saha, D., Martuza, R.L., and Rabkin, S.D. (2017). Macrophage Polarization Contributes to Glioblastoma Eradication by Combination Immunovirotherapy and Immune Checkpoint Blockade. Cancer Cell *32*, 253–267.e5.
36. Colgrove, R.C., Liu, X., Griffiths, A., Raja, P., Deluca, N.A., Newman, R.M., Coen, D.M., and Knipe, D.M. (2016). History and genomic sequence analysis of the herpes simplex virus 1 KOS and KOS1.1 sub-strains. Virology *487*, 215–221.
37. Jackson, J.W., Hancock, T.J., LaPrade, E., Dogra, P., Gann, E.R., Masi, T.J., Panchanathan, R., Miller, W.E., Wilhelm, S.W., and Sparer, T.E. (2019). The Human Cytomegalovirus Chemokine vCXCL-1 Modulates Normal Dissemination Kinetics of Murine Cytomegalovirus *In Vivo*. MBio *10*, e01289-19.
38. Tuzmen, C., Cairns, T.M., Atanasiu, D., Lou, H., Saw, W.T., Hall, B.L., Cohen, J.B., Cohen, G.H., and Glorioso, J.C. (2020). Point Mutations in Retargeted gD Eliminate the Sensitivity of EGFR/EGFRvIII-Targeted HSV to Key Neutralizing Antibodies. Mol. Ther. Methods Clin. Dev. *16*, 145–154.